

COMMERCIAL ABSORPTION CHILLER MODELS FOR EVALUATION OF CONTROL STRATEGIES

Eric A. Koepfel
Student Member ASHRAE

Sanford A. Klein, Ph.D.
Member ASHRAE

John W. Mitchell, Ph.D., P.E.
Fellow ASHRAE

ABSTRACT

A steady-state computer simulation model of a direct-fired double-effect water-lithium bromide absorption chiller in the parallel-flow configuration was developed from first principles. Unknown model parameters such as heat transfer coefficients were determined by matching the model's calculated state points and coefficient of performance (COP) against nominal full-load operating data and COPs obtained from a manufacturer's catalog. The model compares favorably with the manufacturer's performance ratings for varying water circuit (chilled and cooling) temperatures at full-load conditions and for chiller part-load performance. The model was used (1) to investigate the effect of varying the water circuit flow rates with the chiller load and (2) to optimize chiller part-load performance with respect to the distribution and flow of the weak solution.

INTRODUCTION

On-peak electrical energy and demand charges have contributed to an increasing interest in absorption chillers. Direct-fired (natural gas) double-effect absorption chillers using water-lithium bromide are most commonly used for commercial cooling applications. These absorption chillers have a larger first cost than electric chillers but they can be cost-effective in the long term, depending on the electric and gas rates and rebates offered by utilities.

Absorption chillers require electrical energy to operate the chiller pumps, the cooling tower fans, and the chilled- and cooling-water pumps. An absorption chiller rejects more energy than an electric chiller and therefore requires larger cooling-water flow rates, which increases the pumping and cooling tower electrical requirements. Field monitoring data indicate that the parasitic energy varies between 7% and 11% of the cooling capacity for both a 704-kW (200-ton) and a 1,408-kW (400-ton) double-effect absorption chiller located in Wisconsin for the month of August 1993. This is a significant energy input cost. For a typical COP of about 1 for these chillers and an electrical energy cost of about four times that of natural gas, the parasitics represent about 40% of the total energy input cost.

Research on absorption chillers has focused mainly on the design and analysis of the components comprising the chiller and not on optimization of the system operation of the chiller with the cooling tower and the external water circuits (chilled and cooling water). It is important to investigate the system performance of the chiller and its supervisory controls to reduce these parasitics and improve the total chiller economics. Bedard (1993) investigated varying the cooling-water flow rate and inlet cooling (exiting tower) water temperature for a single-effect absorption chiller and concluded that varying the cooling-water flow rate can be done inexpensively and safely, resulting in significant savings.

Vliet et al. (1982) simulated a double-effect water-lithium bromide absorption chiller in series-flow configuration. Gomed and Grossman (1990) used the computer simulation code developed by Grossman and Michelson (1985) and Grossman et al. (1987) to investigate the performance of chillers of both series- and parallel-flow configurations. Both studies investigated the chiller performance as a function of various design and operational variables. The model presented here differs from the above-mentioned models in that it was developed with the intention of replicating manufacturer performance ratings for both full- and part-load conditions. The model can then be used to predict chiller performance under different operating conditions resulting from using alternative control strategies.

The objective of this work is to develop a steady-state computer simulation model of a direct-fired, double-effect water-lithium bromide absorption chiller in the parallel-flow configuration. The cycle configuration of the model is similar to that of a leading manufacturer. The unknown parameters in the model (heat transfer coefficients) were determined by matching the model's calculated state points and COP against nominal full-load operating data and COP obtained from a manufacturer's catalog (YAS 1992, 1993) and from Aizawa et al. (1981). The model was then compared to the manufacturer's performance ratings for a range of water circuit temperatures at full load and for chiller part-load performance. After the comparisons were found to be satisfactory, the model was used to investigate the effect of varying the water-circuit flow rates with the chiller load and to optimize

Eric A. Koepfel is a research assistant and Sanford A. Klein and John W. Mitchell are professors of mechanical engineering in the Solar Energy Laboratory at the University of Wisconsin, Madison.

chiller part-load performance with respect to the distribution and flow of the weak solution.

MODEL DESCRIPTION

The chiller modeled is a direct-fired, double-effect water-lithium bromide absorption chiller in parallel-flow configuration (Figure 1). The solid lines in Figure 1 represent the solution flow and the dashed lines represent the refrigerant flow. The overall model consists of component models for the evaporator, condenser, low- and high-temperature generators, low- and high-temperature solution heat exchangers, absorber, mixer, splitter, expansion valves, and pumps. For discussion of the cycle, the concentration refers to the lithium bromide concentration on a weight basis (percentage), and model points are given in brackets. The parallel-flow arrangement splits the weak solution (3), sending a fraction to the high-temperature generator and the rest to the low-temperature generator. Heat is supplied to the high-temperature generator to boil off the refrigerant-water (17). This water vapor then condenses in the low-temperature generator (18), boiling off more water (7), thus creating the "double effect." The strong solutions leaving the two generators (14, 21) are mixed together (4) before entering the absorber, where the concentrated solution absorbs the water vapor and rejects heat to the cooling water. The cooling-water circuit (22-25) is shown in Figure 1 and is a series flow in which the cooling water first enters the absorber, then the condenser, and is then sent to a cooling tower. The chilled-water circuit (26, 27) is also shown in Figure 1.

A float valve is located on the inlet of the high-temperature generator (not shown in Figure 1). As the chiller unloads, the concentration in the high-temperature generator decreases. Due to the rise in the solution level, the float valve decreases the amount of solution sent to the high-temperature generator. Therefore, the parallel-flow split (PFS = $[11]/[3]$) will decrease, as will the weak solution flow rate due to the increased head. This information regarding the float valve was recorded by Bedard (1994). The float valve is not modeled directly; rather, a relationship between the parallel-flow split and the solution concentration is obtained.

A steady-state computer simulation model of the chiller was written using an equation-solver program (Klein and Alvarado 1993). Property data for water were provided by the program, and the properties of the water-lithium bromide solution were obtained from correlations given in ASHRAE (1993). The model input data available from the manufacturer's catalog are the cooling load (Q_{cool}), the chilled- and cooling-water flow rates, and the inlet cooling-water (22) and leaving chilled-water (27) temperatures.

The adjustable model parameters include the overall heat transfer coefficient/area product (UA) values for the evaporator, condenser, low-temperature generator, low- and high-temperature solution heat exchangers, and absorber; the parallel-flow split (PFS) between points 11 and 3; high-temperature generator combustion efficiency; and the weak solution volumetric flow rate, $V(1)$.

Given the load, the model determines the required energy input to the high-temperature generator. The COP is

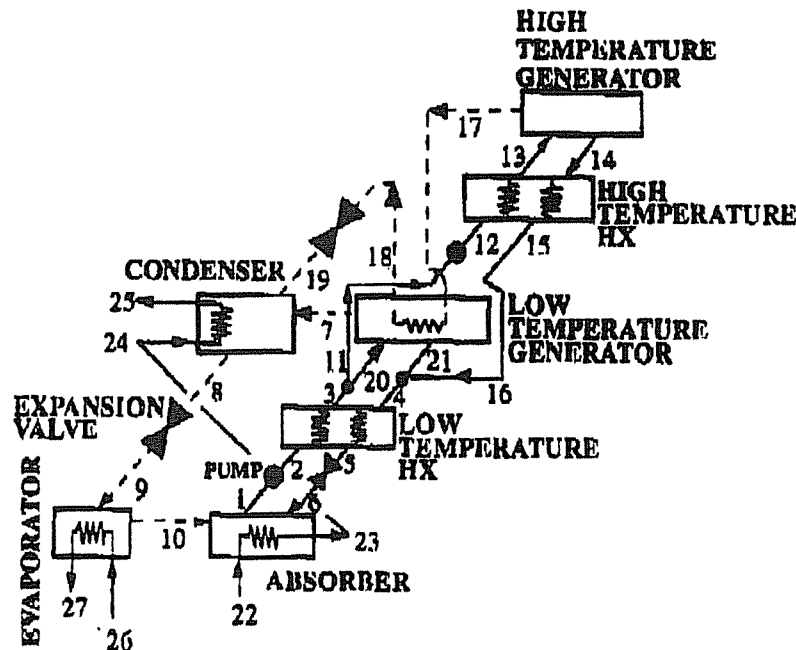


Figure 1 Model diagram of a double-effect absorption chiller in parallel-flow configuration. Solid lines represent the solution flow; broken lines represent the refrigerant flow.

calculated on the basis of the higher heating value (HHV) of methane. The following assumptions were employed in the model

- No internal heat or pressure losses.
- The high pressure is set by the refrigerant condensing in the low-temperature generator. The intermediate pressure is set by the refrigerant condensing in the condenser, and the low pressure is set by the evaporating refrigerant.
- The refrigerant out of the evaporator is saturated vapor. The refrigerant out of the low-temperature generator is saturated liquid. The refrigerant out of the condenser is saturated liquid.
- The solution in the two generators and the absorber is in equilibrium with the state of the refrigerant.
- The superheated vapor (17) leaving the high-temperature generator is in equilibrium with the incoming weak solution (13). As a result, the superheated temperature (17) is lower than the exiting strong solution temperature (14), as observed in actual cycle operating data.
- The above also applies to the superheated vapor leaving the low-temperature generator.
- Components that exchange energy are modeled as counterflow heat exchangers.
- There is perfect mixing in the absorber.
- The system is operating at steady-state conditions.

Mass and energy balance equations were written for each of the components, along with the appropriate equilibrium equations. All heat transfer rates are expressed as a function of a log-mean temperature difference. Generalized equations used in the model are summarized next. (In the following equations, i refers to enthalpy.)

Mass balance equations:

Total mass balance:

$$\sum \dot{m}_{in} - \sum \dot{m}_{out} = 0 \quad (1)$$

Total LiBr mass balance:

$$\sum (x_{in} \dot{m}_{in}) - \sum (x_{out} \dot{m}_{out}) = 0 \quad (2)$$

Energy balance equations:

$$\dot{Q} + \sum (\dot{m}_{in} i_{in}) - \sum (\dot{m}_{out} i_{out}) = 0 \quad (3)$$

Rate equations:

$$\dot{Q} = UA \Delta T_{lm, counterflow} \quad (4)$$

Equilibrium equations for the generators/absorber:

Water-LiBr solution:

$$T = f(P, x) \quad (5)$$

and

$$i = f(T, x) \quad (6)$$

Exiting superheated vapor:

$$T = f(P, x) \quad (7)$$

and

$$i = f(T, P) \quad (8)$$

A two-phase mixture can occur as the weak solution is throttled to the absorber pressure (6). The quality, temperature, liquid concentration, and liquid and vapor enthalpies of the two-phase mixture of point (6) are calculated in the model. The flashing of the refrigerant from the solution of point (5) was not directly accounted for. Using the calculated values, the energy consequence of the flashing was checked and determined to be minimal, but the solution is closer to the possibility of crystallization if flashing does occur.

FULL-LOAD PERFORMANCE OF THE CHILLER MODEL

The absorber, evaporator, condenser, low-temperature generator, and low- and high-temperature solution heat exchangers were modeled as counterflow heat exchangers. The UA values of these heat exchangers could not be determined from first principles, as the component geometry and the dimensions are unknown. There are nine degrees of freedom in the model due to the six unknown UA values (absorber, condenser, evaporator, low-temperature generator, and low- and high-temperature solution heat exchangers), a parallel-flow split parameter ($PFS = [11]/[3]$), high-temperature generator combustion efficiency, and weak solution volumetric flow rate, $V(1)$. These nine parameters were determined by matching the model's calculated state points and COP against nominal full-load operating data and COPs obtained from a manufacturer's catalog and from Aizawa et al. (1981). The matching was done for a 1,408-kW (400-ton) chiller with a leaving chilled-water temperature of 6.7°C (44°F) and an inlet cooling-water temperature of 29.4°C (85°F). The water-circuit flow rates were obtained from the manufacturer's catalog. The chilled-water flow rate was 60.6 L/s (961 gpm), and the cooling-water flow rate was 115.6 L/s (1,832 gpm).

This matching was done by first specifying concentrations at three locations, thereby reducing the number of degrees of freedom to six. These specified values are the strong solution concentration leaving the high-temperature generator, $x(14)$, 63.8%; the weak solution concentration entering the high-temperature generator, $x(13)$, 58.3%; and the strong solution concentration entering the absorber, $x(6)$, 62.7%.

The exiting combustion gas temperature, 232.2°C (450°F), and the approximate percentage of excess air were obtained from the manufacturer's catalog. Assuming an inlet

air and gas temperature of 25°C (77°F), a full-load combustion efficiency (HHV) of 0.81 was calculated that reduced the degrees of freedom to five. This combustion efficiency was used to calculate the cycle COP at full load. The remaining five degrees of freedom in the model were reduced by matching the model COP with the catalog COP and by matching as closely as possible the temperatures in the cycle with catalog data, including the leaving cooling-water temperature.

The results are given in Table 1. The weak solution temperature into the high-temperature generator, T(13), is 11°C (19.8°F) lower and the condenser temperature, T(8), is slightly lower than that reported by the manufacturer. All other points compare well with the manufacturer's data. Given the unknown accuracy of the manufacturer's data and the assumptions employed in the model, the results are very good. The parameters determined by the match are given in Table 2. The UA values and the parallel-flow split are not unique. A different set of parameters may have resulted in similar performance.

TABLE 1
Model and Manufacturer Full-Load Operating
Values for a 1,408 kW (400 ton) Chiller

	Units	Model	Manufacturer
COP-HHV		0.92	0.92
x(1)	%	58.3	58.3
x(4)	%	61.7	61.8
x(6)	%	62.7	62.7
x(14)	%	63.8	63.8
T(1)	°C (°F)	39.0 (102.2)	38.0 (100.4)
T(5)	°C (°F)	61.0 (141.8)	60.0 (140.0)
T(8)	°C (°F)	36.8 (98.2)	40.0 (104.0)
T(10)	°C (°F)	4.2 (39.6)	4.0 (39.2)
T(13)	°C (°F)	115.0 (239.0)	126.0 (258.8)
T(14)	°C (°F)	157.0 (314.6)	150.0-155.0 (302.0-311.0)
T(24)	°C (°F)	33.5 (92.3)	33.3 (91.9)
T(25)	°C (°F)	35.0 (95.0)	35.0 (95.0)
T(26)	°C (°F)	12.2 (54.0)	12.2 (54.0)
P _{high}	kPa (mmHg)	79.85 (598.9)	74.6-81.3 (560.0-610.0)
P _{intermediate}	kPa (mmHg)	6.2 (46.5)	6.7 (50.0)
P _{low}	kPa (mmHg)	.82 (6.2)	0.8 (6.0)

TABLE 2
Parameters Determined from the Full-Load Match of a
1,408 kW (400 ton) Chiller

UA Values	kW/K	Btu/ (min·°F)
Evaporator	300	9,479
Condenser	275	8,689
Absorber	160	5,035
Low-temperature generator	48	1,517
High-temperature HX	11	348
Low-temperature HX	18	569
Parallel-flow split, PFS = 0.48		
Weak solution	L/s	gpm
Volumetric flow rate, V(1)	5.2	82.1

VARYING THE WATER-CIRCUIT TEMPERATURES AT FULL LOAD

Also contained in the manufacturer's catalog is the performance rating of the chiller as the leaving chilled-water temperature and inlet cooling-water temperature are varied at full-load conditions. The leaving chilled-water temperature is usually a setpoint for the chiller, and it is monitored in order to modulate the load and maintain a constant leaving chilled-water temperature. The nominal leaving chilled-water temperature is 6.7°C (44°F). The chilled-water flow rate is constant; therefore, the inlet chilled-water temperature varies according to the load. The inlet cooling-water temperature is externally controlled by the cooling tower. The nominal inlet cooling-water temperature is 29.4°C (85°F). The cooling-water flow rate is also constant; therefore, the leaving cooling-water temperature will vary due to the load.

The manufacturer's performance ratings for varying chilled- and cooling-water temperatures were first used to validate the model. Then the performance ratings for varying inlet cooling-water temperatures were used to obtain a relationship between the parallel-flow split and the concentration difference of the high-temperature generator, Δx , where Δx is the difference between the nominal full-load concentration value of 63.8% and the calculated value of the concentration, x(14). This relationship was developed to account for the float valve in the high-temperature generator.

Lowering the inlet cooling-water temperature seems to be an attractive and easily implemented control algorithm for most chiller systems, subject to the ambient wet-bulb temperature. The chiller COP increases progressively as the inlet cooling water temperature is lowered. Lowering the inlet cooling water temperature will significantly lower the

intermediate and high pressures, thereby allowing the amount of water vapor produced in the low-temperature generator to increase and thereby improve chiller efficiency. The manufacturer recommends that the temperature not be lowered below 21.1°C (70°F). As explained by Bedard (1993), this limit is not due to crystallization concerns, but rather the weak solution becomes so dilute that it will deplete the refrigerant supply. It is the rate of descent in the cooling-water temperature, not the absolute temperature, that is of concern.

The results of varying the inlet cooling-water temperature for the model of the 1,408-kW (400-ton) chiller are given in Figure 2. The load, the water-circuit flow rates, the weak solution volumetric flow rate, $V(1)$, and the UA values are held constant for all three cases. It is assumed that the heat transfer coefficients for the water side do not vary due to the temperature changes. For case 1, the combustion efficiency and the parallel-flow split were held constant at the nominal full-load values of 0.81 and 0.48. In case 2, the combustion efficiency increased 3% from the nominal 29.4°C (85°F) to 21.1°C (70°F). This adjustment was determined by having the exiting combustion gas temperature vary in proportion to the high-temperature generator temperature, $T(14)$. It was assumed that the amount of air would decrease in proportion with the fuel, thereby increasing the heat exchanger effectiveness and decreasing the exiting combustion gas temperature. Due to the lower fuel flow rate and the lower exiting temperature, the combustion efficiency will increase. As seen in Figure 2, the model shows the same trend and compares favorably with the catalog information. Similar trends for the inlet cooling-water temperature were obtained by Vliet et al. (1982) and Gomed and Grossman (1990).

For full-load conditions, the model shows that the chiller can be operated at lower inlet cooling-water temperatures. The strong solution concentration, $x(14)$, decreases linearly as the inlet cooling-water temperature is lowered, and this decrease in concentration moves the cycle away from the crystallization region.

The small differences between the calculated COP (for case 2) and the manufacturer's data were eliminated by using the model to determine the parallel-flow split to match COPs. From the match, a relationship between the parallel-flow split and the concentration difference, Δx , was developed, which will be used to model the float valve in the high-temperature generator:

$$PFS = m[11]/m[3] = 0.48 - 0.014\Delta x \quad (9)$$

The calculated COP using this relationship and a varying combustion efficiency results in the performance shown as case 3 in Figure 2. The weak solution flow rate will also decrease as a result of the increased head, but the volumetric flow rate was assumed to remain constant due to the lack of information on the pump.

The leaving chilled-water temperature was also varied,

and the results are shown in Figure 3 for both case 1 and case 3. Again, the load, the weak solution volumetric flow rate, $V(1)$, the water-circuit flow rates, and the UA values are held constant. For case 3, the combustion efficiency varied only slightly (0.07%) and Equation 9 was used for the parallel-flow split. For case 1, the parallel-flow split and combustion efficiency were constant at 0.48 and 0.81, respectively. The model results of case 3 show the same trend, but slightly under predict the effect of increasing the leaving chilled-water temperature reported by the manufacturer. A maximum 2% difference results at a temperature of 8.9°C (48°F)

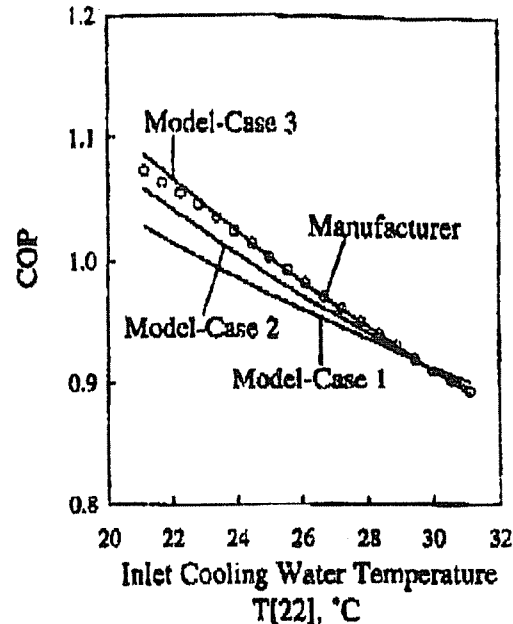


Figure 2 Results of varying the inlet cooling-water temperature at full load. The UA values, water-circuit flow rates, and solution volumetric flow rate, $V(1)$, are constant. Case 1—constant combustion efficiency and parallel-flow split. Case 2—varying combustion efficiency, constant parallel-flow split. Case 3—varying combustion efficiency and parallel-flow split.

PART-LOAD PERFORMANCE OF THE CHILLER

The part-load performance of any chiller is important since chillers most often operate at part-load conditions. Catalog information indicates that absorption chillers are designed so that the greatest efficiency is obtained at between 50% and 100% of full load. The part-load control is obtained by modulating the fuel to the high-temperature generator. In the model, it is assumed that the weak solution volumetric flow rate, $V(1)$, is constant, the parallel-flow split varies according to Equation 9, and the combustion efficiency varies in proportion to the high-temperature generator temperature. The leaving chilled-water temperature is 6.7°C (44°F) and the inlet cooling-water temperature is

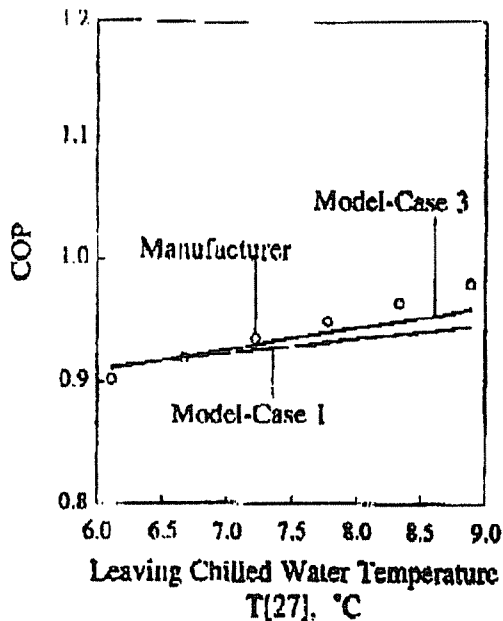


Figure 3 Results of varying the leaving chilled-water temperature at full load. The UA values, water-circuit flow rates, and solution volumetric flow rate, $V(1)$, are constant. Case 1—constant combustion efficiency and parallel-flow split. Case 3—varying combustion efficiency and parallel-flow split.

29.4°C (85°F). The chilled- and cooling-water flow rates are also constant at 60.6 L/s (961 gpm) and 115.6 L/s (1832 gpm), respectively. The load was varied for the above-mentioned conditions for the case of constant UA values and for the case in which the UA values for the evaporator, condenser, low-temperature generator, and high-temperature solution heat exchanger varied due to the decreasing refrigerant mass flow rates ([17], [8], [9]) and solution mass flow rates ([12], [14]) as the unit unloads. Since the solution flow rate out of the absorber is constant, the UA values for the low-temperature solution heat exchanger and the absorber were held constant. Also, as determined by Greiter et al. (1993), the heat transfer coefficient for the solution side of the absorber was taken to be independent of the solution flow rate.

For evaporation of refrigerant sprayed on the outside of horizontal tubes, the heat transfer coefficient for turbulent flow is given by Chun and Seban (1971) as

$$h = 0.0038 Re^{0.4} Pr^{0.5} \left(\frac{k^3 g \rho^2}{\mu^2} \right)^{1/3} \quad (10)$$

For both condensation of refrigerant on the outside of horizontal tubes and condensation of refrigerant inside horizontal tubes, the heat transfer coefficient is given by Kern (1950) as

$$h = 1.5 \left(\frac{mC}{LN_p \mu} \right)^{-1/3} \left(\frac{k^3 g \rho^2}{\mu^2} \right)^{1/3} \quad (11)$$

For turbulent flow in circular tubes, the heat transfer coefficient can be determined from the Dittus-Boelter correlation, as given by Incropera and DeWitt (1990):

$$h = \left(\frac{k}{D} \right) 0.023 Re^{0.8} Pr^n \quad (12)$$

Using the foregoing relations for the heat transfer coefficients and assuming the wall heat transfer resistance to be negligible, the UA values were rewritten in terms of constants and the appropriate mass flow rates as

$$UA_{evap} = \frac{1}{\frac{1}{C_1 m [10]^a} + C_2} \quad (13)$$

$$UA_{cond} = \frac{1}{\frac{1}{C_3 m [8]^{1/3}} + C_4} \quad (14)$$

$$UA_{low\ gen} = \frac{1}{\frac{1}{C_5 m [17]^{-1/3}} + C_6} \quad (15)$$

and

$$UA_{high\ HX} = UA_{high\ HX, nom} \left(\frac{m [12]}{m [12]_{nom}} \right)^b \quad (16)$$

It is assumed that the transport properties are constant. The constants in Equations 13, 14, 15, and 16 were solved at the nominal full-load condition by equating Equations 13, 14, and 15 to the nominal full-load UA values and by equating the heat transfer resistances on each side of the heat exchanger.

The results for the part-load performance are given in Figure 4. The COP is plotted as a function of the part-load factor, which is the cooling capacity, Q_{evap} , divided by the nominal capacity. The model COP for both constant and varying UA values only increases slightly between a part-load factor of 0.80 and 1.0, where the manufacturer's COP increases more significantly. At a part-load factor of 0.30, at which point the chiller will cycle off, the model COP for the case of varying UA values differs from the manufacturer's COP by a maximum value of 5.9%. The exact causes for the difference between calculated and catalog part-load performance are not known. The difference may be due to several factors, including model assumptions, inaccuracy in the UA values, assumption of a constant weak solution volumetric flow rate, and modeling of the parallel-flow split by Equation 9. However, the differences between catalog and model COPs are small, and the model displays the correct trends so that it is judged to be satisfactory for the control studies for which it was developed.

The part-load data could have been used in determining some of the UA values and the parallel-flow split relationship for the float valve. It was decided instead to use nominal full-load operating data and full-load performance

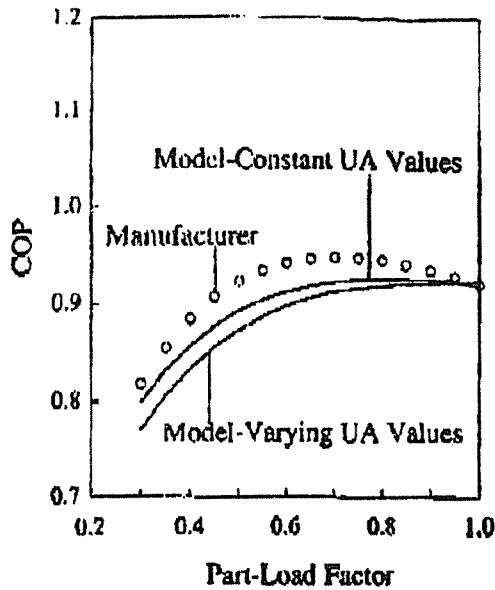


Figure 4 Model and manufacturer part-load performance. UA values vary due to the decreasing flow rates of the refrigerant and the solution.

ratings to match the model's performance and to determine unknown parameters. The nominal full-load operating data and COP are available from most manufacturers, and the part-load performance rating is available from only one manufacturer. The model could be used to predict chiller part-load performance at nominal and off-design conditions for other double-effect configurations for which catalog data are not available.

The model part-load performance for a range of inlet cooling water temperatures was investigated. It was discovered that the operating parameters have interacting effects on the COP. For example, a normalized COP as a function of the load for an inlet cooling water temperature of 29.4°C (85°F) was obtained from the model. Also obtained from the model was a normalized COP as a function of the inlet cooling water temperature (based on full-load conditions). The normalized COP functions were used to calculate chiller part-load COP at various inlet cooling-water temperatures other than the nominal, but they did not give the same performance as the model. Rather, the functions under predicted the model performance, especially at lower part-load factors and cooling-water temperatures, with differences up to a maximum of 13%.

VARYING THE WATER-CIRCUIT FLOW RATES

The effect of varying the chilled- and cooling-water flow rates at chiller part-load performance was investigated. A constant temperature difference of 5.6°C (10°F) is maintained and the flow rate is varied as a result of the load change. To account for the varying water-circuit flow rates,

the UA values were rewritten, using Equation 12, as

$$UA_{evap} = \frac{1}{\frac{1}{C_1 m [10]^{-2}} + \frac{1}{C_7 V_{chill}^{-0.5}}} \quad (17)$$

$$UA_{cond} = \frac{1}{\frac{1}{C_3 m [2]^{-1/3}} + \frac{1}{C_8 V_{cool}^{-0.8}}} \quad (18)$$

and

$$UA_{abs} = \frac{1}{C_{10} + \frac{1}{C_9 V_{cool}^{-0.8}}} \quad (19)$$

The constants in Equations 17, 18, and 19 were determined in the same manner as previously discussed, by equating these equations with the corresponding nominal full-load UA values and by equating the two heat transfer resistances.

The results of varying the water-circuit flow rates are given in Figure 5. The COP is plotted as a function of the part-load factor. The chilled- and cooling-water flow rates are varied separately. The base case of constant flow rates (Figure 4, varying UA values) is also plotted for comparison. Varying the chilled-water flow rate results in negligible COP changes, whereas varying the cooling-water flow rate results in a decrease in the COP. A maximum 11% difference exists at a part-load factor of 0.30. The effect of vary-

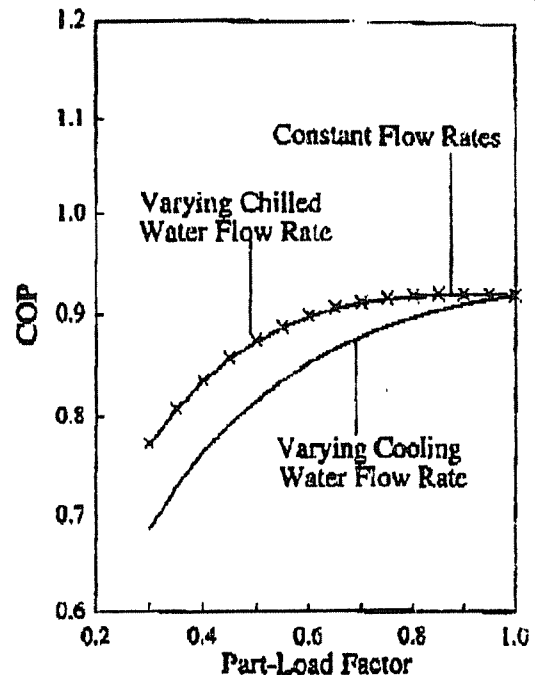


Figure 5 Model results of varying the chilled- and cooling-water flow rates with the load.

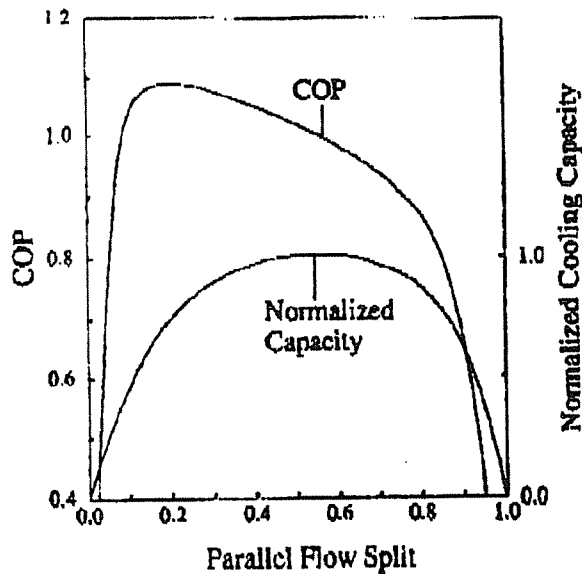


Figure 6 Model results of varying the parallel-flow split at constant solution volumetric flow rate, $V(1)$, and high-temperature generator temperature, $T(14)$.

ing the chilled- and cooling-water flow rates was reported by Vliet et al. (1982) to be negligible and minor, respectively.

From the results of Figure 5, varying the water-circuit flow rates with the load seems to be an attractive control option, since the flow rates and the associated pumping requirements can be drastically reduced with a small effect on chiller COP. Varying the water-circuit flow rates more than 25% is not currently recommended by the manufacturer. In order for the flow rates to be varied, additional safety controls would be needed to ensure safe operation. However, it was concluded by Bedard (1993) that the flow rates can be varied safely and inexpensively through the use of microprocessor controls.

PART-LOAD OPTIMIZATION

The nominal full-load parallel-flow split was determined to be 0.48. The model performance as a function of the parallel-flow split was investigated by varying the split while the weak solution volumetric flow rate, $V(1)$, and the high-temperature generator temperature, $T(14)$, were held constant at the corresponding nominal full-load values. The UA values varied according to Equations 13 through 16. The water-circuit flow rates are constant. The results are given in Figure 7, with the COP and normalized cooling capacity, $(Q_{evap}/Q_{evap,nom})$, plotted as a function of the parallel-flow split. The results of Figure 7 are similar to the results obtained by Gommé and Grossman (1990), except that the capacity curve is not as flat and insensitive to the parallel-flow split. The optimal-flow split (PFS) for maxi-

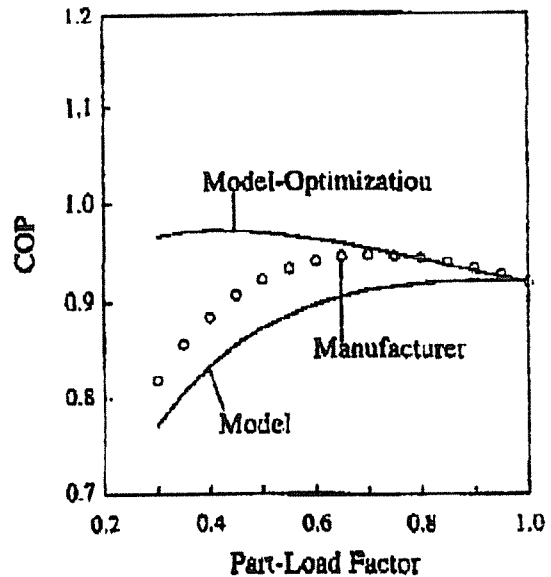


Figure 7 Model result of optimizing the chiller COP with respect to the parallel-flow split, and varying the weak solution volumetric flow rate, $V(1)$.

imum COP is about 0.20, lower than the optimal value of 0.25 found by Gommé and Grossman (1990). The optimal-flow split (PFS) for maximum capacity is about 0.55. The optimal split (PFS) without sacrificing capacity is about 0.43, which is higher than the value of 0.30 reported by Gommé and Grossman (1990). Although there are differences between the two models, the trends are similar.

The model's part-load performance was maximized with respect to the parallel-flow split. This was done by inputting the high-temperature generator temperature, $T(14)$, as a function of the part-load factor and maximizing the COP. The high-temperature generator temperature was provided (from model output) to maintain a reasonable temperature for the optimization. To provide the extra degree of freedom, the weak solution volumetric flow rate, $V(1)$, was allowed to vary. The UA value for the low-temperature solution heat exchanger was varied in the same manner as in Equation 16 due to the varying flow rate. From this optimization, a curve fit of the normalized parallel-flow split (PFS/PFS_{nom}) as a function of Δx was obtained. The normalized weak solution volumetric flow rate ($V(1)/V(1)_{nom}$) was fit in terms of ΔPFS , where ΔPFS is the difference between the nominal parallel-flow split and the calculated value of the parallel-flow split. The weak solution volumetric flow rate was fit in terms of the change in the parallel-flow split because the change will influence the pump head and therefore the flow rate. The curve fits were input into the model to obtain the results in Figures 7 and 8.

In Figure 7, the COP, as a result of varying the parallel-flow split and the weak solution volumetric flow rate according to the fits obtained from the optimization, is plot-

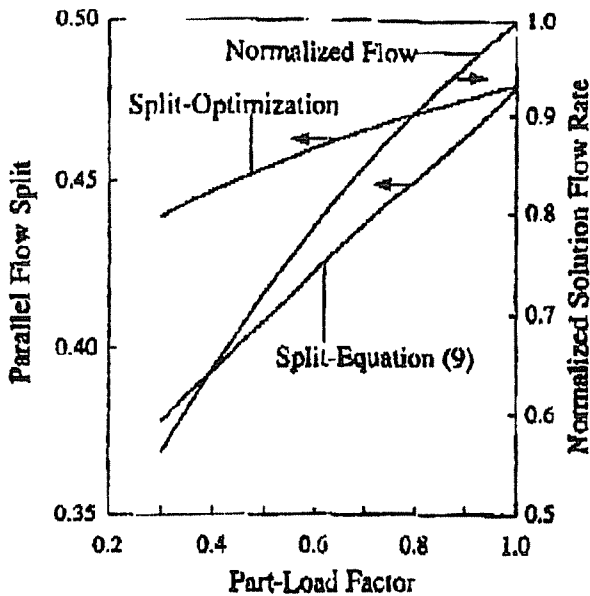


Figure 8 The parallel-flow split and normalized solution volumetric flow rate, $V(1)/V(1)_{nom}$, as a function of the load, for the optimization and that used by the model.

ted. Also plotted in Figure 7 are the manufacturer's data and the model performance that used Equation 9 for the parallel-flow split and a constant solution volumetric flow rate. The COP from the optimization gradually increases and only slightly decreases at a part-load factor of 0.40. The COP is significantly higher than the model and the manufacturer's data at lower part-load factors. The parallel-flow split and the normalized solution volumetric flow rate for the optimization are plotted in Figure 8, along with the parallel-flow split using Equation 9. The parallel-flow split from the optimization decreases less significantly than that from using Equation 9, and the solution volumetric flow rate decreases as it should with the part-load factor.

The calculated results indicate that the COP at part-load conditions could be improved by controlling the parallel-flow split and the solution flow rate in an optimal manner.

CONCLUSIONS

A steady-state computer simulation model of a direct-fired, double-effect water-lithium bromide absorption chiller in parallel-flow configuration compares favorably with a manufacturer's catalog information. The calculated performance due to lowering the inlet cooling-water temperature at full-load conditions agrees with the catalog's performance. Model performance of increasing the leaving chilled-water temperature at full-load conditions slightly under predicts the catalog performance. For chiller part-load performance, the model differs from the catalog data by a maximum of 6% at a part-load factor of 0.30. The effect of

varying the chilled-water flow rate at part load is negligible, whereas varying the cooling-water flow rate results in a maximum 11% lower COP. The model is judged satisfactory for use in control studies of varying the water-circuit temperatures and flow rates and can be used for predicting chiller performance at off-design conditions for which performance data are not available. The optimization of the chiller part-load performance with respect to the distribution of the weak solution between the two generators and a varying weak solution volumetric flow rate has been shown to significantly improve chiller COP.

Field monitoring data have shown the parasitic energy of a direct-fired (natural gas) double-effect water-lithium bromide absorption chiller to be significant in terms of the energy input cost. The system performance of an absorption chiller with a cooling tower and the water circuits will be investigated with the model described in this paper in order to optimize the total system performance.

ACKNOWLEDGMENTS

This study was sponsored by the Wisconsin Center for Demand-Side Research, a consortium of Wisconsin Gas and Electric Utilities, the Public Service Commission, and the university.

NOMENCLATURE

- () = model state point
- C = numerical constant
- COP = coefficient of performance
- D = tube diameter (m [ft])
- g = gravitational acceleration
- h = heat transfer coefficient ($W/(m^2 \cdot K)$, $Btu/(h \cdot ft^2 \cdot ^\circ F)$)
- HHV = higher heating value of fuel (MJ/m^3 [Btu/ft^3])
- HX = heat exchanger
- i = enthalpy (kJ/kg [Btu/lb_m])
- k = thermal conductivity ($W/(m \cdot K)$; $Btu/(h \cdot ft \cdot ^\circ F)$)
- L = length of tube (m [ft])
- m = mass flow rate (kg/s [lb_m/min])
- n = numerical constant
- N_t = number of tubes
- P = pressure (kPa [mmHg])
- PFS = parallel-flow split
- ΔPFS = nominal parallel-flow split minus the calculated parallel-flow split
- Pr = Prandtl number
- Q = heat transfer rate (kW [Btu/h])
- Re = Reynolds number
- T = temperature ($^\circ C$ [$^\circ F$])
- ΔT_{lm} = log-mean temperature difference ($^\circ C$ [$^\circ F$])
- UA = product of the overall heat transfer coefficient and the area (kW/K , $Btu/(min \cdot ^\circ F)$)
- V = volumetric flow rate (L/s [gpm])

x = LiBr concentration on weight basis (%)
 Δx = 63.8 $\Delta x(14)$

Greek Symbols

μ = absolute viscosity (mPa·s; lb_m/[ft·h])
 ρ = density (kg/m³ [lb_m/ft³])

Subscripts

abs = absorber
evap = evaporator
chill = chilled water
cond = condenser
cool = cooling water
low gen = low-temperature generator
high HX = high-temperature solution heat exchanger
nom = nominal

REFERENCES

- Aizawa, M., M. Nagao, and W. Kazuo. 1981. Direct-fired absorption chiller-heater. *Hitachi Review* 30(1): 19-24.
- ASHRAE. 1993. *1993 ASHRAE handbook—Fundamentals*, pp. 17.82-17.83. Atlanta: American Society of Heating, Refrigerating and Air-Conditioning Engineers, Inc.
- Bedard, G.S. 1993. Varied flow rate applications for commercial absorption chillers. *AES-Vol. 31, Proceedings of the International Heat Pump Conference*, New Orleans, LA, January 19-21, pp. 133-139. New York: American Society of Mechanical Engineers.
- Bedard, G.S. 1994. Personal communication.
- Chun, K.R., and R.A. Schan. 1971. Heat transfer to evaporating liquid films. *ASME Journal of Heat Transfer*, Nov., pp. 371-396.
- Gommed, K., and G. Grossman. 1990. Performance analysis of staged heat pumps: Water-lithium bromide systems. *ASHRAE Transactions* 96(1): 1590-1598.
- Greiter, I., A. Wagner, V. Weiss, and G. Alefeld. 1993. Experimental investigation of heat and mass transfer in a horizontal-tube falling film absorber with aqueous solutions. *AES-Vol. 31, Proceedings of the International Heat Pump Conference*, New Orleans, LA, January 19-21, pp. 225-232. New York: American Society of Mechanical Engineers.
- Grossman, G., and E. Michelson. 1985. A modular computer simulation of absorption systems. *ASHRAE Transactions* 91(2B): 1808-1827.
- Grossman, G., K. Gommed, and D. Gadoth. 1987. A computer model for simulation of absorption systems in flexible and modular form. *ASHRAE Transactions* 93(2): 2389-2428.

- Incropera, F.P., and D.P. DeWitt. 1990. *Fundamentals of heat and mass transfer*. New York: John Wiley & Sons.
- Kern, D.Q. 1950. *Process heat transfer*. New York: McGraw-Hill.
- Klein, S.A., and F.L. Alvarado. 1993. *EES—Engineering equation solver*. Middleton, WI: F-Chart Software.
- Vliet, G.C., M.B. Lawson, and R.A. Lithgow. 1982. Water-lithium bromide double-effect absorption cooling cycle analysis. *ASHRAE Transactions* 88(1): 811-823.
- YAS. 1992. Form 155.17-EG1 (291). York, PA: York International Corporation.
- YAS. 1993. Form 155.17-EG3 (493). York, PA: York International Corporation.